

The first low-mass stars: critical metallicity or dust-to-gas ratio?

Raffaella Schneider^{1*}, Kazuyuki Omukai², Simone Bianchi³, Rosa Valiante³

¹ *INAF/Osservatorio Astronomico di Roma, Via di Frascati 33, 00040 Monteporzio, Roma, Italy*

² *Department of Physics, Kyoto University, Kyoto 606-8502, Japan*

³ *INAF/Osservatorio Astrofisico di Arcetri, Largo Enrico Fermi 5, 50125 Firenze, Italy*

September 2011

ABSTRACT

We explore the minimal conditions which enable the formation of metal-enriched solar and sub-solar mass stars. Using a one-zone semi-analytical model, we accurately follow the chemical and thermal evolution of the gas with the aim of understanding how the initial metal and dust content alters the cooling and fragmentation properties, hence the characteristic stellar mass. We find that in the absence of dust grains, gas fragmentation occurs at densities $n_{\text{H}} \sim [10^4 - 10^5] \text{ cm}^{-3}$ when the metallicity exceeds $Z \sim 10^{-4} Z_{\odot}$. The resulting fragmentation masses are $\geq 10 M_{\odot}$. The inclusion of Fe and Si cooling does not affect the thermal evolution as this is dominated by molecular (mostly OH, H₂O and CO) cooling even for metallicities as large as $Z = 10^{-2} Z_{\odot}$. The presence of dust is the key driver for the formation of low-mass stars. We focus on three representative core-collapse supernova (SN) progenitors (a $Z = 0$ star with $20 M_{\odot}$ and two $Z = 10^{-4} Z_{\odot}$ stars with $20 M_{\odot}$ and $35 M_{\odot}$), and consider the effects of reverse shocks of increasing strength: these reduce the depletion factors, $f_{\text{dep}} = M_{\text{dust}} / (M_{\text{dust}} + M_{\text{met}})$, alter the shape of the grain size distribution function and modify the relative abundances of grain species and of metal species in the gas phase. We find that the lowest metallicity at which fragmentation occurs is $Z = 10^{-6} Z_{\odot}$ for gas pre-enriched by the explosion of a $20 M_{\odot}$ primordial SN ($f_{\text{dep}} \geq 0.22$) and/or by a $35 M_{\odot}$, $Z = 10^{-4} Z_{\odot}$ SN ($f_{\text{dep}} \geq 0.26$); it is ~ 1 dex larger, when the gas is pre-enriched by a $Z = 10^{-4} Z_{\odot}$, $20 M_{\odot}$ SN ($f_{\text{dep}} \geq 0.04$). Cloud fragmentation depends on the depletion factor and it is suppressed when the reverse shock leads to a too large destruction of dust grains. These features are all consistent with the existence of a minimum dust-to-gas ratio, \mathcal{D}_{cr} , above which fragmentation is activated. We derive a simple analytic expression for \mathcal{D}_{cr} which depends on the total grain cross-section per unit mass of dust; for grain composition and properties explored in the present study, $\mathcal{D}_{\text{cr}} = [2.6 - 6.3] \times 10^{-9}$. When the dust-to-gas ratio of star forming clouds exceeds this value, the fragmentation masses range between $0.01 M_{\odot}$ and $1 M_{\odot}$, thus enabling the formation of the first low-mass stars.

Key words: Cosmology: galaxies: evolution, stars: formation, Population II, ISM: abundances, dust

1 INTRODUCTION

The formation of the first low-mass and long-lived stars marks an important step in cosmic evolution. Despite that a large fraction of the Galactic Halo has now been surveyed (Beers & Christlieb 2005; Helmi 2008), no evidence for the existence of primordial low-mass stars has been found to date. The most primitive star of the Galactic Halo has a $[\text{Fe}/\text{H}] = -4.99$ and, contrary to other extremely iron-poor

stars, shows no carbon, nitrogen or oxygen enhancement, resulting in a total metallicity of $Z = 4.5 \times 10^{-5} Z_{\odot}$ (Caffau et al. 2011).

This lends support to the idea that the formation of solar or sub-solar mass stars¹ requires some minimal conditions which do not rely on carbon and oxygen line-cooling

¹ For WMAP7 cosmological parameters, the current Hubble time is $t_{\text{H}} = 13.75$ Gyr (Jarosik et al. 2011). Depending on the stellar initial metallicity, this corresponds to the lifetime of stars with masses in the range $[0.7 - 0.9] M_{\odot}$ (Raiteri et al. 1996)

* E-mail: raffaella.schneider@oa-roma.inaf.it

(Frebel, Johnson, and Bromm 2007) and that can operate at very low but non-zero metallicity (Schneider et al. 2003, 2006).

This empirical evidence is supported by a solid theoretical argument: the micro-physics of the H_2 molecule, the only available coolant in $\sim 10^6 M_\odot$ mini-halos at $z \sim 20-30$, sets a characteristic thermodynamic state where gravitational fragmentation of star-forming clouds is halted, which corresponds to a minimum Jeans mass of $\sim 500 M_\odot$ (see Bromm et al. 2009 and references therein). Simulations starting from cosmological initial conditions have confirmed that vigorous fragmentation of collapsing clouds does not occur (Abel, Bryan & Norman 2002; Bromm, Coppi & Larson 2002; Yoshida et al. 2006; Yoshida, Omukai & Hernquist 2008), although there have been evidences for the formation of massive binary systems (Turk, Abel, O’Shea 2009).

The subsequent phase of gas accretion onto the central proto-stellar core is subject to radiative feedback effects from the growing protostar which leads to a plausible but uncertain range of final stellar masses, $[30 - 100] M_\odot$ (Omukai & Palla 2003; Tan & McKee 2004; Bromm & Loeb 2004; Yoshida et al. 2008; McKee & Tan 2008; Hosokawa & Omukai 2009; Ohkubo et al. 2009). The accretion disk may become susceptible to fragmentation, forming groups of protostars (Machida et al. 2008; Stacy, Greif & Bromm 2010; Clark et al. 2011; Greif et al. 2011), but current simulations are not able to follow the subsequent interactions of group members with the surrounding gas cloud.

Rotation, turbulence and magnetic fields are known to play an important role in present-day star formation and their importance in the first star forming regions at high redshift still needs to be fully assessed (see e. g. Schleicher et al. 2009; Clark et al. 2011b and references therein). Whether or not these additional physical processes might enable the formation of low-mass Pop III stars remains an open question.

Here we follow a different approach: guided by the observed constancy of the stellar characteristic mass in the local Universe, $M_{\text{ch}} \sim 0.3 M_\odot$ (for recent reviews see Elmegreen 2009; Bastian, Covey & Meyer 2010), which has been interpreted to originate from the minimum Jeans mass imprinted during gravitational fragmentation (Li, Klessen & McLow 2003; Larson 2005; Jappsen et al. 2005; Elmegreen, Klessen & Wilson 2008), we explore the most extreme environmental conditions where low-mass star formation can occur in the first mini-halos at high redshifts.

The transition in the characteristic stellar mass, often referred to as Pop III/II transition, has been explored by many authors. On the relatively small scale of a single star forming cloud, semi-analytic and numerical studies have emphasized the role of metals and dust.

The effects of metal-line cooling, predominantly by O, C, Si and Fe, are relevant at relatively low densities, $\leq [10^4 - 10^5] \text{ cm}^{-3}$, before and around the onset of NLTE-LTE transition of the corresponding level populations. When the initial metallicity of the star forming cloud exceeds a critical value of $Z_{\text{cr}} \sim [10^{-4} - 10^{-3}] Z_\odot$, the minimum Jeans mass achieved by gravitational fragmentation is found to vary in the range $[10 - 100] M_\odot$, depending on the presence/absence of molecular coolants in the chemical network and on the number of heating/cooling processes included in the modelling (Omukai 2000; Bromm et al. 2001; Schnei-

der et al. 2002; Bromm & Loeb 2003; Santoro & Shull 2006; Jappsen et al. 2007, 2009; Smith, Sigurdsson & Abel 2008; Hocuk & Spaans 2010). In this case, the formation of sub-solar or solar mass stars, which may survive to the present time, is determined during the subsequent evolutionary phases, by gas accretion within each clump and dynamical interactions within the cluster (Machida et al. 2009; Omukai, Hosokawa & Yoshida 2010).

As in present-day conditions, thermal emission by collisionally excited dust grains is an efficient cooling channel at high densities, $\geq [10^{12} - 10^{14}] \text{ cm}^{-3}$. As a result, the typical Jeans masses which can be achieved by gravitational fragmentation are much smaller, $[0.01 - 1] M_\odot$ (Schneider et al. 2003, 2006; Omukai et al. 2005; Tsuribe & Omukai 2006; Clark, Glover & Klessen 2008; Omukai et al. 2010; Dopcke et al. 2011). Thus, efficient dust-cooling leads to a transition in the characteristic mass by several orders of magnitude with respect to the primordial case. The metallicity at which this transition takes place depends on the dust depletion factor, defined as,

$$f_{\text{dep}} = \frac{M_{\text{dust}}}{M_{\text{dust}} + M_{\text{met}}}, \quad (1)$$

where M_{dust} and M_{met} are the dust and gas-phase metals masses, respectively.

In the model presented in Omukai et al. (2005), where we assumed present-day ISM composition and grain properties, $f_{\text{dep}} = 0.49$ (Pollack et al. 1994) and the onset of dust-induced cooling and fragmentation leading to the formation of $\sim 1 M_\odot$ fragments starts to be effective when $10^{-6} Z_\odot < Z_{\text{cr}} \leq 10^{-5} Z_\odot$. This result has been confirmed by numerical simulations (Tsuribe & Omukai 2006, 2008; Clark et al. 2008; Omukai et al. 2010; Dopcke et al. 2011).

Since the properties of dust grains at high redshifts might be different with respect to those observed locally, in Schneider et al. (2006) we have investigated the dust-driven transition under the hypothesis that the collapsing star-forming cloud had been pre-enriched by metal-free core-collapse supernova (with a progenitor of $22 M_\odot$) and by a pair-instability supernova (with a progenitor of $195 M_\odot$). The adopted metal composition and dust-grain properties were computed according to the model of dust nucleation in supernova ejecta developed by Todini & Ferrara (2001) and by Schneider, Salvaterra & Ferrara (2003). The depletion factors were $f_{\text{dep}} = 0.23$ (for the $22 M_\odot$ progenitor) and $f_{\text{dep}} = 0.65$ (for the $195 M_\odot$) and low-mass fragmentation was found to occur already at $Z_{\text{cr}} = 10^{-6} Z_\odot$.

An important confirmation of a Pop III/II transition driven by dust cooling has been recently provided by Caffau et al. (2011), who have reported the observation of a Galactic Halo star with $Z = 4.5 \times 10^{-5} Z_\odot$. Since this paper has appeared at the time of submission of the present work, we defer a specific analysis of this particular star to a future study.

Here we intend to investigate the effects of varying the initial f_{dep} on the gravitational collapse and fragmentation properties of pre-enriched star forming clouds. The questions we intend to address are: (i) what is the minimum fragment mass that can be achieved by metal-line cooling? and (ii) What is the minimum dust depletion factor to activate dust-induced cooling? To answer these questions, we first calculate the thermal evolution of collapsing gas clouds

that cool only through molecular (H_2 , HD, H_2O , CO, OH) and metal (CI, CII, OI, SiII, FeII) line cooling. Then, we use the model developed by Bianchi & Schneider (2007) to compute the mass, composition and size distribution of dust formed in the ejecta of a few representative SN progenitors. Starting from these initial conditions, we take into account the partial destruction of the newly formed dust by the SN reverse shock. In particular, we consider reverse shocks of increasing strength, assuming increasingly large circumstellar densities. Following the models by Bianchi & Schneider (2007) we can control the reduction of the depletion factor (more than 80% of the initial dust mass is destroyed) in a self-consistent way and explore the implications for the fragmentation properties of pre-enriched star forming clouds.

The plan of the paper is as follows: in Section 2 we present the model; in Section 3 we discuss the thermal evolution driven by line-cooling and the resulting fragmentation properties. In Section 4 we describe the adopted model grid of core-collapse SN progenitors and the associated dust properties. In Section 5 we present the thermal evolution and fragmentation of clouds pre-enriched by these explosions. In Section 6 we discuss the results and, finally, in section 7 we summarize our main conclusions.

2 THE MODEL

The thermal and chemical evolution of collapsing gas clouds is investigated using the model presented in Omukai (2000) and in Omukai et al. (2005) with CO, H_2O and OH cooling rates recently modified as in Omukai et al. (2010). As a new feature of the code, we have included the contribution of Fe and Si to metal-line cooling. Here we briefly summarize the features of the model which are relevant for the purposes of the present study and we refer the interested reader to the original papers for a thorough description of the code.

The temperature evolution is computed by solving the energy equation,

$$\frac{de}{dt} = -p \frac{d}{dt} \frac{1}{\rho} - \Lambda_{\text{net}} \quad (2)$$

where the pressure, p , and the specific thermal energy, e , are given by,

$$p = \frac{\rho k T}{\mu m_{\text{H}}} \quad (3)$$

$$e = \frac{1}{\gamma - 1} \frac{k T}{\mu m_{\text{H}}} \quad (4)$$

and ρ is the central density, T is the temperature, γ is the adiabatic exponent, μ is the mean molecular weight² and m_{H} is the mass of hydrogen nuclei.

The terms on the right-hand side of the energy equation are the compressional heating rate,

$$\frac{d\rho}{dt} = \frac{\rho}{t_{\text{col}}} \quad \text{with} \quad t_{\text{col}} = \frac{1}{\sqrt{1 - f_{\text{p}}}} \sqrt{\frac{3\pi}{32G\rho}}, \quad (5)$$

² The mean molecular weight is 1.23 for a fully atomic gas and 2.29 for a fully molecular gas.

where f_{p} is the ratio between pressure gradient to gravity (see Omukai et al. 2005 for the expression) and the net cooling rate, Λ_{net} , which consists of three components,

$$\Lambda_{\text{net}} = \Lambda_{\text{line}} + \Lambda_{\text{cont}} + \Lambda_{\text{chem}}. \quad (6)$$

The first component, Λ_{line} , represents the cooling rate due to the emission of line radiation, which includes molecular line emission of H_2 , HD, OH, H_2O and CO (Omukai et al. 2010) and atomic fine-structure line emission. In addition to CI, CII and OI (Omukai et al. 2005), here we have considered the contribution of Fe and Si lines (see section 3 below). The second component, Λ_{cont} , represents the cooling rate due to the emission of continuum radiation, which includes thermal emission by dust grains and H_2 collision-induced emission. The last term, Λ_{chem} , indicates the cooling/heating rate due to chemical reactions. When the gas cloud is optically thick to a specific cooling radiation, the cooling rate is correspondingly reduced by multiplying by the photon escape probability (see Omukai 2000).

We do not consider the effects of the Cosmic Microwave Background (CMB) radiation field, which provides a redshift dependent effective temperature floor (Clarke & Bromm 2003; Omukai et al. 2005). At $z \geq 10 - 15$, the evolution of star-forming clouds can be significantly affected but only at relatively large metallicities, $Z \geq 10^{-2} Z_{\odot}$ (Smith et al. 2009; Schneider & Omukai 2010). We will return to this point in section 6.

The effects of dust grains on the thermal evolution are due to (i) dust thermal emission and (ii) the increased formation rate of H_2 on its surface and (iii) the heating associated to the latter process. The treatment of these physical processes is the same as in Schneider et al. (2006). Here we report only the fundamental equations which regulate dust thermal emission and refer the interested reader to Schneider et al. (2006) for further details.

2.1 Dust cooling

Dust grains affect the thermal evolution of the collapsing gas cloud when the energy transfer between gas and dust due to collisions is radiated away. Dust thermal emission rate can be expressed as,

$$\Lambda_{\text{gr}} [\text{erg/s/gr}] = 4 \sigma T_{\text{gr}}^4 \kappa_{\text{P}} \beta_{\text{esc}} \frac{\rho_{\text{gr}}}{\rho}, \quad (7)$$

where σ is the Stefan-Boltzmann constant, T_{gr} is the dust temperature, κ_{P} is the Planck mean opacity of dust grains per unit dust mass, β_{esc} is the photon escape probability, and the dust mass density, ρ_{gr} , can be expressed as $\rho \mathcal{D}$, with \mathcal{D} indicating the dust-to-gas ratio. Following Omukai (2000), the photon escape probability can be written as,

$$\beta_{\text{esc}} = \min(1, \tau^{-2}) \quad \text{with} \quad \tau = \kappa_{\text{P}} \rho \lambda_{\text{J}}, \quad (8)$$

where the optical depth is estimated across one local Jeans length (roughly the size of the central core region in the Penston-Larson similarity solution). The Planck mean opacity per unit dust mass is,

$$\kappa_{\text{P}} = \frac{\pi}{\sigma T_{\text{gr}}^4} \int_0^{\infty} B_{\nu}(T_{\text{gr}}) \kappa_{\nu} d\nu \quad (9)$$

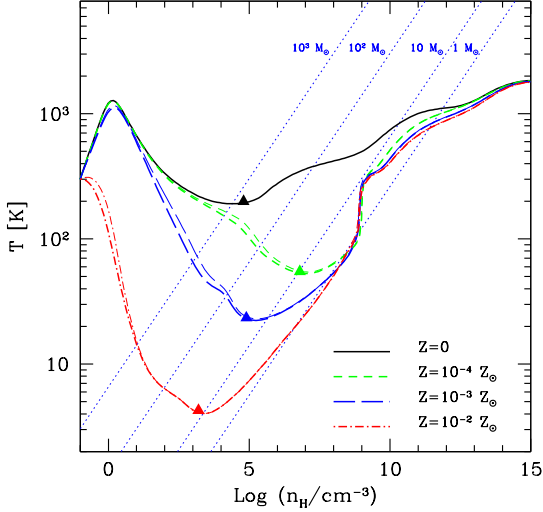


Figure 1. Thermal evolution of collapsing clouds with initial metallicities $Z = 0, 10^{-4}Z_{\odot}, 10^{-3}Z_{\odot}, 10^{-2}Z_{\odot}$, from top to bottom. For each of the $Z > 0$ models, two lines are shown: the thin one represents the prediction of the Omukai et al. (2005) model; the thick one shows the effects of including [FeII] and [SiII] cooling. The diagonal dotted lines indicate locii of constant Jeans masses, as labelled in the figure, and the points with triangles mark the states where fragmentation conditions are met (see text).

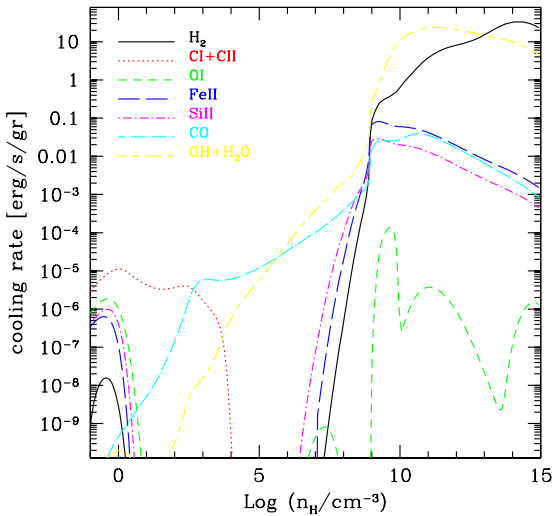


Figure 2. Individual metal fine-structure lines (FeII, SiII, ClI+Cl, OI) and molecular lines (H_2 , CO, OH+ H_2O) contributions to the cooling rate of a gas cloud with initial metallicity $Z = 10^{-2}Z_{\odot}$ (see Fig.1).

where κ_{ν} is the absorption coefficient for the frequency ν per unit dust mass and $B_{\nu}(T_{\text{gr}})$ is the Planck brightness (see Schneider et al. 2006).

The dust temperature, T_{gr} , is determined by the balance between dust thermal emission and the dust heating rate due to collisions with gas particles (Hollenbach & McKee 1979), $H_{\text{gr}} = \rho\Lambda_{\text{gr}}$, with

$$H_{\text{gr}}[\text{erg/s/cm}^3] = \frac{n_{\text{gr}}(2kT - 2kT_{\text{gr}})}{t_{\text{coll}}}, \quad (10)$$

where $t_{\text{coll}}^{-1} = n_{\text{H}}\sigma_{\text{gr}}\bar{v}_{\text{H}}f$ is the average time between two successive collisions, n_{gr} and σ_{gr} are the grain number density and cross section, \bar{v}_{H} is the average speed of hydrogen nuclei and $f = \bar{n}v/n_{\text{H}}\bar{v}_{\text{H}} \approx 0.395$ measures the contribution of other species³.

In the density range where collisional dust heating is relevant ($n_{\text{H}} > 10^{12-13} \text{cm}^{-3}$), it is a good approximation to assume that the gas is fully molecular and follows a Maxwellian distribution so that,

$$\bar{v}_{\text{H}} = \left(\frac{8kT}{\pi m_{\text{H}}}\right)^{1/2}. \quad (11)$$

If we further write,

$$n_{\text{gr}}\sigma_{\text{gr}} = n_{\text{H}}m_{\text{H}}(1 + 4y_{\text{He}})SD \quad (12)$$

in eq. (10), where S is the total grain cross section per unit mass of dust, the equation $\rho\Lambda_{\text{gr}} = H_{\text{gr}}$ appears to be independent of the dust-to-gas ratio. Thus, T_{gr} depends only on gas temperature and density and on grain specific properties (cross section and mean opacity, see Schneider et al. 2006 for further details).

3 FRAGMENTATION BY METAL-COOLING: EFFECTS OF FE AND SI LINES

In this section, we discuss the thermal evolution of collapsing gas clouds when only molecules and metals contribute to the cooling rate in eq. (6). Thus, we assume that no dust is present. For simplicity, we adopt an ISM with the solar elemental composition (Anders & Grevesse 1989) and the mass of each element is decreased proportionally to the total metallicity.

To estimate the effects of FeII and SiII lines on gas cooling, we do not solve the full Fe and Si chemistry (as we do for the other elements) but we simply assume that all the Fe and Si contributes to cooling. Fig. 1 shows the thermal evolution of collapsing gas clouds with varying initial metallicities ($Z = 0, 10^{-4}Z_{\odot}, 10^{-3}Z_{\odot}, 10^{-2}Z_{\odot}$, from top to bottom). For the $Z > 0$ models, thin lines represent the predictions obtained with Omukai et al. (2005) models and thick lines show the current models with the inclusion of SiII and FeII line-cooling. As it is apparent from the figure, the difference is very small and confined to the density range $n_{\text{H}} < 10^6 \text{cm}^{-3}$. In fact, even for the highest metallicity model that we have considered, $Z = 10^{-2}Z_{\odot}$, the cooling rate is dominated by molecular lines, specifically by H_2O and OH. This is shown

³ Since we are interested in very low gas metallicities ($10^{-7}Z_{\odot} \leq Z \leq 10^{-4}Z_{\odot}$) we can safely neglect the contribution of heavy elements and write $f = 0.3536 + 0.5y_{\text{He}}$ with $y_{\text{He}} = n_{\text{He}}/n_{\text{H}} = 0.083$, which corresponds to a He mass fraction of $Y=0.25$.

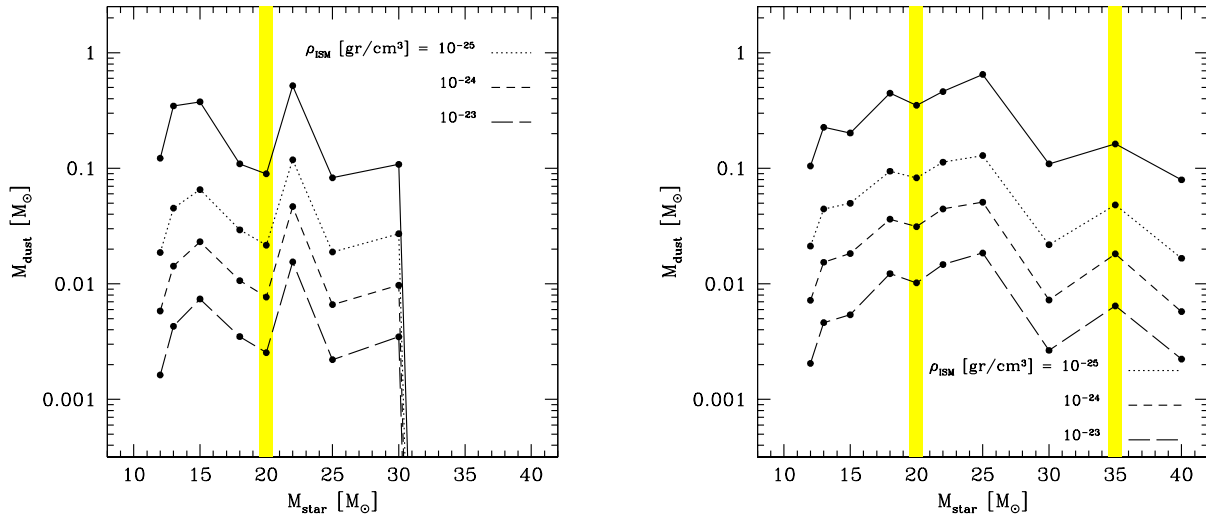


Figure 3. Mass of dust predicted by SN as a function of the progenitor stellar mass for two initial metallicities: $Z = 0$ (left panel) and $Z = 10^{-4}Z_{\odot}$ (right panel). In each panel, the solid line refers to the mass of dust predicted at the end of the condensation phase (**norev**) and for the **rev1**, **rev2**, **rev3** cases (dotted, dashed, long-dashed lines, respectively) corresponding to ISM densities of 10^{-25} , 10^{-24} and 10^{-23} gr/cm^{-3} , respectively.

Table 1. Ejecta composition of the three SN models; for each of these we show the depletion factor, f_{dep} (first column), the mass of dust grains, M_{dust} (second column), the total mass of gas-phase metals, M_{met} (third column) and the mass of O and C atoms (fourth and fifth columns, respectively) in the **norev**, **rev1**, **rev2**, and **rev3** cases. All masses are in solar units. The last column shows the total dust cross section per unit dust mass (see section 2.1).

| SN progenitor | models | f_{dep} | M_{dust} | M_{met} | M_{O} | M_{C} | S [$10^5 \text{ cm}^2/\text{gr}$] |
|--------------------------------------|--------------|-----------------------|-----------------------|-----------------------|-----------------------|-----------------------|-------------------------------------|
| $Z = 0, 20 M_{\odot}$ | norev | 0.91 | 8.96×10^{-2} | 8.93×10^{-3} | 8.92×10^{-3} | 0 | 4.71 |
| | rev1 | 0.22 | 2.16×10^{-2} | 7.69×10^{-2} | 8.92×10^{-3} | 6.8×10^{-2} | 5.24 |
| | rev2 | 7.81×10^{-2} | 7.69×10^{-3} | 9.08×10^{-2} | 8.92×10^{-3} | 8.19×10^{-2} | 5.37 |
| | rev3 | 2.58×10^{-2} | 2.54×10^{-3} | 9.60×10^{-2} | 8.92×10^{-3} | 8.71×10^{-2} | 5.21 |
| $Z = 10^{-4}Z_{\odot}, 20 M_{\odot}$ | norev | 0.17 | 0.35 | 1.72 | 1.47 | 0 | 2.22 |
| | rev1 | 3.99×10^{-2} | 8.27×10^{-2} | 1.99 | 1.50 | 0.14 | 2.44 |
| | rev2 | 1.51×10^{-2} | 3.13×10^{-2} | 2.04 | 1.50 | 0.19 | 2.50 |
| | rev3 | 4.92×10^{-3} | 1.02×10^{-2} | 2.06 | 1.50 | 0.21 | 2.50 |
| $Z = 10^{-4}Z_{\odot}, 35 M_{\odot}$ | norev | 0.87 | 0.16 | 2.45×10^{-2} | 2.45×10^{-2} | 0 | 2.35 |
| | rev1 | 0.26 | 4.82×10^{-2} | 0.14 | 2.45×10^{-2} | 0.11 | 2.62 |
| | rev2 | 9.70×10^{-2} | 1.82×10^{-2} | 0.17 | 2.45×10^{-2} | 0.14 | 2.68 |
| | rev3 | 3.44×10^{-2} | 6.44×10^{-3} | 0.18 | 2.45×10^{-2} | 0.16 | 2.62 |

in Fig. 2, where we compare the individual contributions to the cooling rate. Although FeII and SiII are the most important coolants among metal fine-structure lines in some density ranges, their contribution to the total cooling rate is smaller than that provided by molecules.

In Fig.1, the diagonal dotted lines represent constant Jeans mass values in the (n_{H}, T) plane. These are computed using the relation,

$$M_{\text{J}} = \rho \lambda_{\text{J}}^3 \quad (13)$$

$$= 1.69 \times 10^3 M_{\odot} \left(\frac{\mu}{1.23} \right)^{-3/2} \left(\frac{T}{200\text{K}} \right)^{3/2} \left(\frac{n_{\text{H}}}{10^4 \text{cm}^{-3}} \right)^{-1/2},$$

where the Jeans length is,

$$\lambda_{\text{J}} = \left(\frac{\pi k_{\text{B}} T}{G \mu m_{\text{H}} \rho} \right)^{1/2}. \quad (14)$$

The points with triangles mark the states where fragmentation conditions are met. Following Schneider & Omukai (2010), we identify the fragmentation epochs by requiring that the adiabatic index becomes $\gamma > 0.97$ after a phase of cooling (where $\gamma < 1$). To eliminate “false” fragmentation points, where γ is less than 1 only for a short period of time, we impose that $\gamma < 0.8$ during the cooling phase preceding

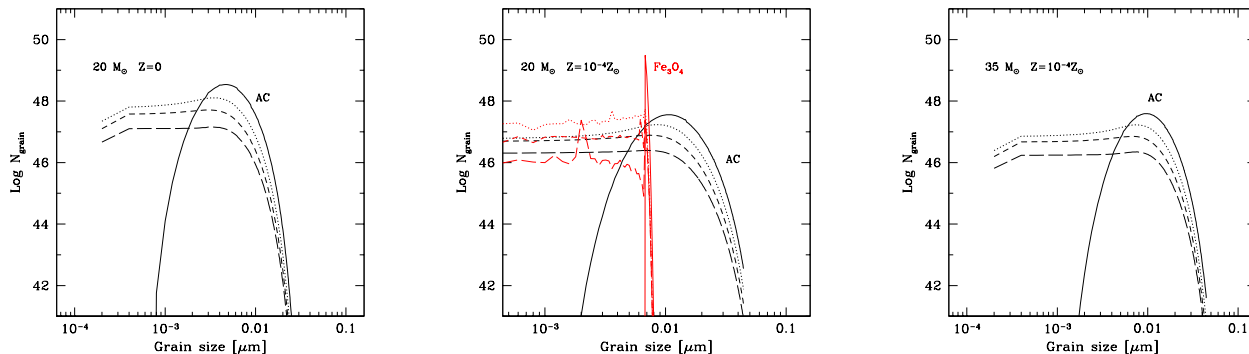


Figure 4. Size distribution function of the dominant dust species resulting from the explosion of a $Z = 0$, $M_{\text{star}} = 20M_{\odot}$ (left panel), $Z = 10^{-4}Z_{\odot}$, $M_{\text{star}} = 20M_{\odot}$ (central panel), and $Z = 10^{-4}Z_{\odot}$, $M_{\text{star}} = 35M_{\odot}$ (right panel). Solid lines show the distribution at the end of the condensation phase (**norev**) and dotted, dashed, long-dashed lines illustrate the effect of reverse shocks with increasing strength (**rev1**, **rev2**, **rev3**, respectively).

the fragmentation epoch (see Schneider & Omukai 2010 for more details).

It is clear from the figure that the minimum fragmentation masses that can be achieved by metal and molecular line-cooling are $\geq 10M_{\odot}$, even for gas clouds with initial metallicity as high as $Z = 10^{-2}Z_{\odot}$. Thus, the additional contribution of Fe and Si lines to the chemical network and cooling rate do not change the main conclusions of previous investigations, based on the model presented in Omukai et al. (2005). In particular, the formation of solar or sub-solar mass fragments requires the presence of dust grains and dust-induced cooling at densities $n_{\text{H}} > 10^{12}\text{cm}^{-3}$.

4 MODEL GRID OF CORE-COLLAPSE SN

Figure 3 shows the masses of dust produced by core collapse SN as a function of the progenitor star mass and initial metallicities equal to $Z = 0$ (left panel) and $Z = 10^{-4}Z_{\odot}$ (right panel). The solid lines show dust masses at the end of the condensation phase (no reverse shock model) according to the model developed by Todini & Ferrara (2001) and revisited by Bianchi & Schneider (2007). Here we refer to the fiducial case, where we assume that the first seed critical dust clusters are formed with a minimum of two monomers and that the sticking coefficient is equal to 1 (we refer to Bianchi & Schneider 2007 for more details). We see that the most massive SN ($M_{\text{star}} > 25M_{\odot}$) are less efficient sources of dust due to the strong fallback of metals during the explosion. This is particularly true for the primordial case, where metal (and therefore dust) production is zero beyond a progenitor stellar mass of $30M_{\odot}$. The dotted, dashed, and long-dashed lines show the masses of dust after the passage of the reverse shock when the surrounding ISM density is assumed to be equal to 10^{-25} , 10^{-24} and $10^{-23}\text{gr/cm}^{-3}$, respectively. The reverse shock is modelled following the prescription of Bianchi & Schneider (2007) and dust destruction is caused by both thermal and non-thermal sputtering (see the original paper for more details). The fraction of the initial dust mass which is destroyed and returns back to the gas phase

increases with the ISM density. Hereafter, we will refer to the ejecta properties at the end of the condensation phase as the **norev** case; with **rev1**, **rev2**, **rev3** cases we will indicate the models with reverse shock of increasing strength (increasing ISM density).

As it is reasonable to expect, the mass of dust released by SN increases with the metallicity of the progenitor stars. We focus here on three representative SN models (highlighted in the figure): a $Z = 0$, $20M_{\odot}$ progenitor ($20M_{\odot}, 0$) and two $Z = 10^{-4}Z_{\odot}$ progenitors with masses of $20M_{\odot}$ ($20M_{\odot}, 10^{-4}Z_{\odot}$) and $35M_{\odot}$ ($35M_{\odot}, 10^{-4}Z_{\odot}$). Table 1 describes the final ejecta composition for these three SN in the **norev**, **rev1**, **rev2** and **rev3** cases. The first column lists the depletion factor, f_{dep} , with values in the range $4.92 \times 10^{-3} \leq f_{\text{dep}} \leq 0.91$, decreasing with reverse shock strength. Thus, the conditions we will explore span the value appropriated for the local ISM ($f_{\text{dep}} = 0.49$) as well as values which are 2 dex smaller. Note that the depletion factors are systematically larger for the ($20M_{\odot}, 0$) and the ($35M_{\odot}, 10^{-4}Z_{\odot}$) SN progenitors, despite the smaller final dust and metal yields with respect to the SN progenitor ($20M_{\odot}, 10^{-4}Z_{\odot}$).

The elemental composition of the ejecta depends on the SN progenitor and reverse shock model. As it can be seen from Table 1, oxygen is always the dominant element at the end of the condensation phase (**norev** cases) and carbon is returned to the gas phase after the partial destruction of graphite grains by the reverse shock (**rev1-rev3** cases). We therefore expect that the thermal properties of gas enriched by these ejecta will depend on f_{dep} due to variations both in the abundance of dust grains and in the composition of gas-phase metals.

The reverse shock significantly affects the grain size distribution function, decreasing the number of larger grains and flattening the distribution towards smaller grain sizes. This is shown in Fig.4 where, for each model, the dominant grain species have been reported. Only amorphous carbon (AC) grains form in the ejecta of the ($20M_{\odot}, 0$) and the ($35M_{\odot}, 10^{-4}Z_{\odot}$) progenitors; additional grain species form in the ejecta of the ($20M_{\odot}, 10^{-4}Z_{\odot}$) progenitor, among

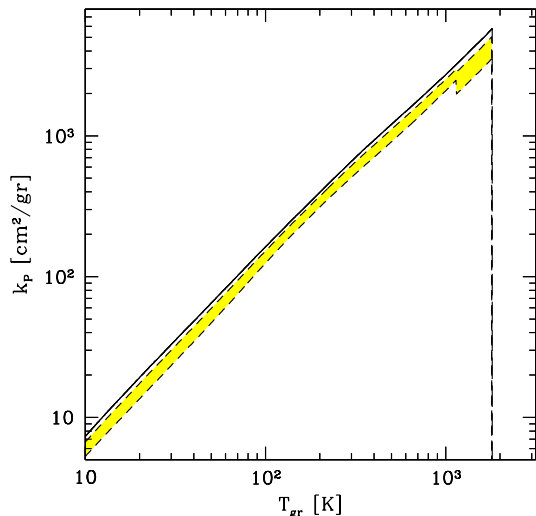


Figure 5. Planck mean opacity per unit dust mass as a function of grain temperature. The solid line refers to models $Z = 0$, $M_{\text{star}} = 20M_{\odot}$, and $Z = 10^{-4}Z_{\odot}$, $M_{\text{star}} = 35M_{\odot}$ which have very similar dust properties. Also, for these two models we only show the opacity at the end of the condensation phase because the passage of the reverse shock has a negligible effect. The dashed region illustrates the maximum (**norev**) and minimum (**rev3**) Planck mean opacity per unit mass for the $Z = 10^{-4}Z_{\odot}$, $M_{\text{star}} = 20M_{\odot}$ model. Line breaks are due to grain sublimation (see text).

which Fe_3O_4 , MgSiO_3 , SiO_2 , and Al_2O_3 (see also Bianchi & Schneider 2007 for more details). Thus, the former two SN progenitors share very similar dust properties. This is reflected by their corresponding grain cross sections per unit dust mass (see the last column in Table 1) and Planck mean opacities (see eq. 9) which are plotted in Fig. 5 as a function of dust grain temperature. The solid lines show the predicted opacity for $(20M_{\odot}, 0)$ and $(35M_{\odot}, 10^{-4}Z_{\odot})$ progenitors with no variations induced by dust destruction in the reverse shock; the shaded region indicates the maximum (**norev** case) and minimum (**rev3** case) Planck mean opacity predicted for the $(20M_{\odot}, 10^{-4}Z_{\odot})$ progenitor. The line breaks are due to grain sublimation, which occurs at a temperature of 1810 K for AC grains and of 1140 K for the additional grain species (Kozasa, Hasegawa, & Nomoto 1989). Since the grain cross section and Planck mean opacity control the efficiency of dust cooling (see Section 2.1), in what follows we restrict the discussion to the most dissimilar SN progenitors, hence a $20M_{\odot}$ star with metallicities $Z = 0$ and $Z = 10^{-4}Z_{\odot}$.

5 RESULTS

In this section we investigate the thermal evolution and fragmentation of collapsing gas clouds enriched by each of the two representative supernova progenitors. We assume that their ejecta uniformly enrich nearby collapsing gas clouds.

Depending on its total gas mass, the collapsing cloud can be enriched to different total metallicities, where by total metallicity we mean the total mass of metals (in the gas-phase and in dust grains) relative to the mass of gas. Figs.6 and 7 show the thermal evolution of a collapsing gas cloud with initial metallicity equal to $10^{-7}Z_{\odot}$, $10^{-6}Z_{\odot}$, $10^{-5}Z_{\odot}$, and $10^{-4}Z_{\odot}$ (from top left to bottom right); in each panel, we plot different reverse shock models varying the depletion factor and the ejecta composition self-consistently (from bottom to top **norev**, **rev1**, **rev2**, **rev3** correspond to solid, dotted, short-dashed and long-dashed lines); as a reference case, the evolution predicted for a $Z = 0$ gas is also shown (top solid line).

The comparison among different panels shows that the deviation from the primordial gas evolution increases with metallicity; when $Z = 10^{-7}Z_{\odot}$, this is limited to relatively large densities, $n_{\text{H}} \geq 10^{12} \text{ cm}^{-3}$, but progressively extends to lower densities as the metallicity increases. At metallicities $10^{-7}Z_{\odot} \leq Z \leq 10^{-4}Z_{\odot}$ the evolution is dominated by dust through both direct cooling (high densities; $\gtrsim 10^{11} \text{ cm}^{-3}$) and increased H_2 cooling due to H_2 formation on dust grains (lower densities; $\lesssim 10^9 \text{ cm}^{-3}$), as already discussed in Omukai et al. (2005) and Schneider et al. (2006). At each given metallicity the largest deviation from the primordial case is associated to the **norev** case, characterized by the largest f_{dep} , and the evolution progressively tend to the primordial limit when lower depletion factors are considered (models **rev1**, **rev2** and **rev3**).

The points with triangles in Figs.6 and 7 mark the states where fragmentation conditions are met. The lowest metallicity at which fragmentation occurs is $Z = 10^{-6}Z_{\odot}$ for the $(20M_{\odot}, 0)$ SN progenitor and it is 1 dex larger, $Z = 10^{-5}Z_{\odot}$, for the $(20M_{\odot}, 10^{-4}Z_{\odot})$ SN progenitor. In both cases, however, cloud fragmentation depends on the depletion factor and it is suppressed when the strength of the reverse shock leads to a too large destruction of dust grains (**rev2** and **rev3** cases).

These features are all consistent with the existence of a minimum dust-to-gas ratio above which fragmentation is activated. Given our definitions of metallicity, Z , and dust depletion factor, f_{dep} , the dust-to-gas ratio can be written as $\mathcal{D} = Z f_{\text{dep}}$. Thus, the minimum \mathcal{D} is reached at a lower total metallicity for models with larger depletion factors, such as the $(20M_{\odot}, 0)$ SN progenitor (see Table 1).

Fig.8 represents the results of all the models investigated so far in a $Z - f_{\text{dep}}$ plane. Empty symbols indicate no fragmentation and filled symbols represent models where fragmentation conditions are met. The solid line marks the border between the no-fragmentation and fragmentation zones and corresponds to a minimum dust-to-gas ratio of only $\mathcal{D}_{\text{cr}} = 4.4 \times 10^{-9}$. At any given metallicity, low-mass fragmentation can be activated when $\mathcal{D} \geq \mathcal{D}_{\text{cr}}$ or $f_{\text{dep}} \geq \mathcal{D}_{\text{cr}}/Z$.

A simple argument for the origin of \mathcal{D}_{cr} runs as follows. The second high-density dip in the thermal evolution of collapsing gas clouds is activated when the energy transfer rate between gas and dust is more efficient than the compressional heating rate due to gravitational contraction, that is,

$$H_{\text{gr}}/\rho > -p \frac{d}{dt} \frac{1}{\rho}. \quad (15)$$

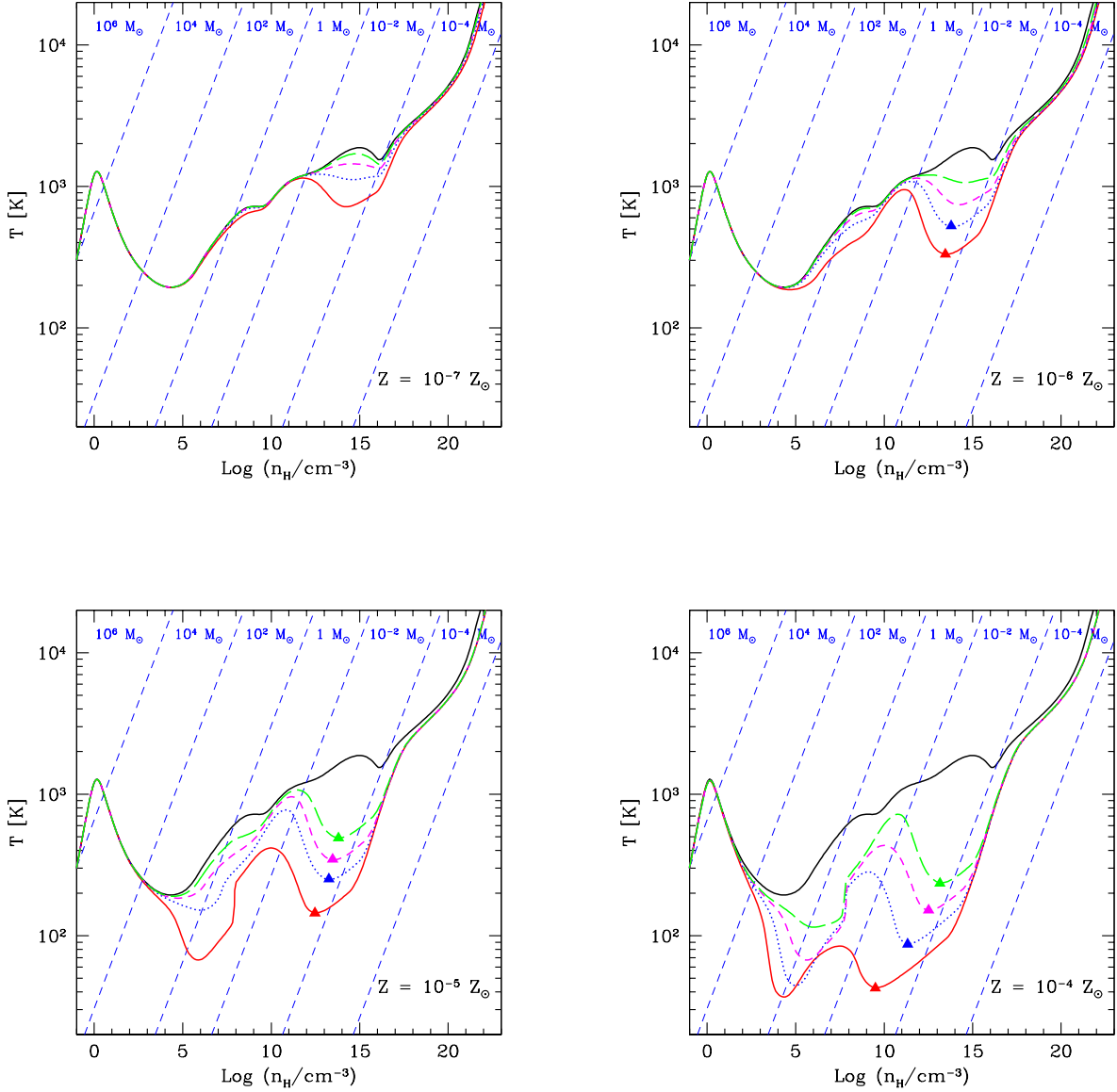


Figure 6. Thermal evolution of clouds enriched by the $(20M_{\odot}, 0)$ SN model. In each panel, we have assumed that the gas has been pre-enriched to a total metallicity of $10^{-7}Z_{\odot}$, $10^{-6}Z_{\odot}$, $10^{-5}Z_{\odot}$, and $10^{-4}Z_{\odot}$ (from top left to bottom right). In each panel, we show the evolution for four values of f_{dep} corresponding to the **novev**, **rev1**, **rev2**, and **rev3** cases (bottom solid, dotted, short-dashed, long-dashed, respectively). For each of these cases, the ejecta composition is varied consistently, as presented in Table 1 and Figs. 4, 5. As a reference model, we also show the evolution predicted for a purely primordial gas cloud (top solid line). The diagonal dashed lines represent lines of constant Jeans mass and the triangles identify the points where fragmentation conditions are met (see text).

Using eqs. (10)-(12) for the left-hand term and eqs. (3)-(5) for the compressional heating rate, eq.(15) leads to a condition on the dust-to-gas ratio times the cross section per unit dust mass,

$$SD > 1.4 \times 10^{-3} \text{cm}^2/\text{gr} \left[\frac{T}{10^3 \text{K}} \right]^{-1/2} \left[\frac{n_{\text{H}}}{10^{12} \text{cm}^{-3}} \right]^{-1/2}, \quad (16)$$

where we have assumed that at the onset of dust cooling, before gas and dust become thermally coupled, $T_{\text{gr}} \ll T$. The above relation has been evaluated at reference gas tem-

perature and density of $T \sim 10^3$ K and $n_{\text{H}} \sim 10^{12} \text{cm}^{-3}$. Indeed, the sharp temperature drop, which activates fragmentation, can be achieved only if dust cooling exceeds the compressional heating rate when $n_{\text{H}} < 10^{12} \text{cm}^{-3}$ and H_2 formation heating keeps the gas temperature at $\sim 10^3$ K. Beyond this density, H_2 becomes fully molecular, chemical heating is no longer effective, and dust-cooling causes only a mild temperature decrease. It follows from eq. (16) that the critical dust-to-gas ratio is inversely proportional to the total grain cross section per unit mass of dust. As it can

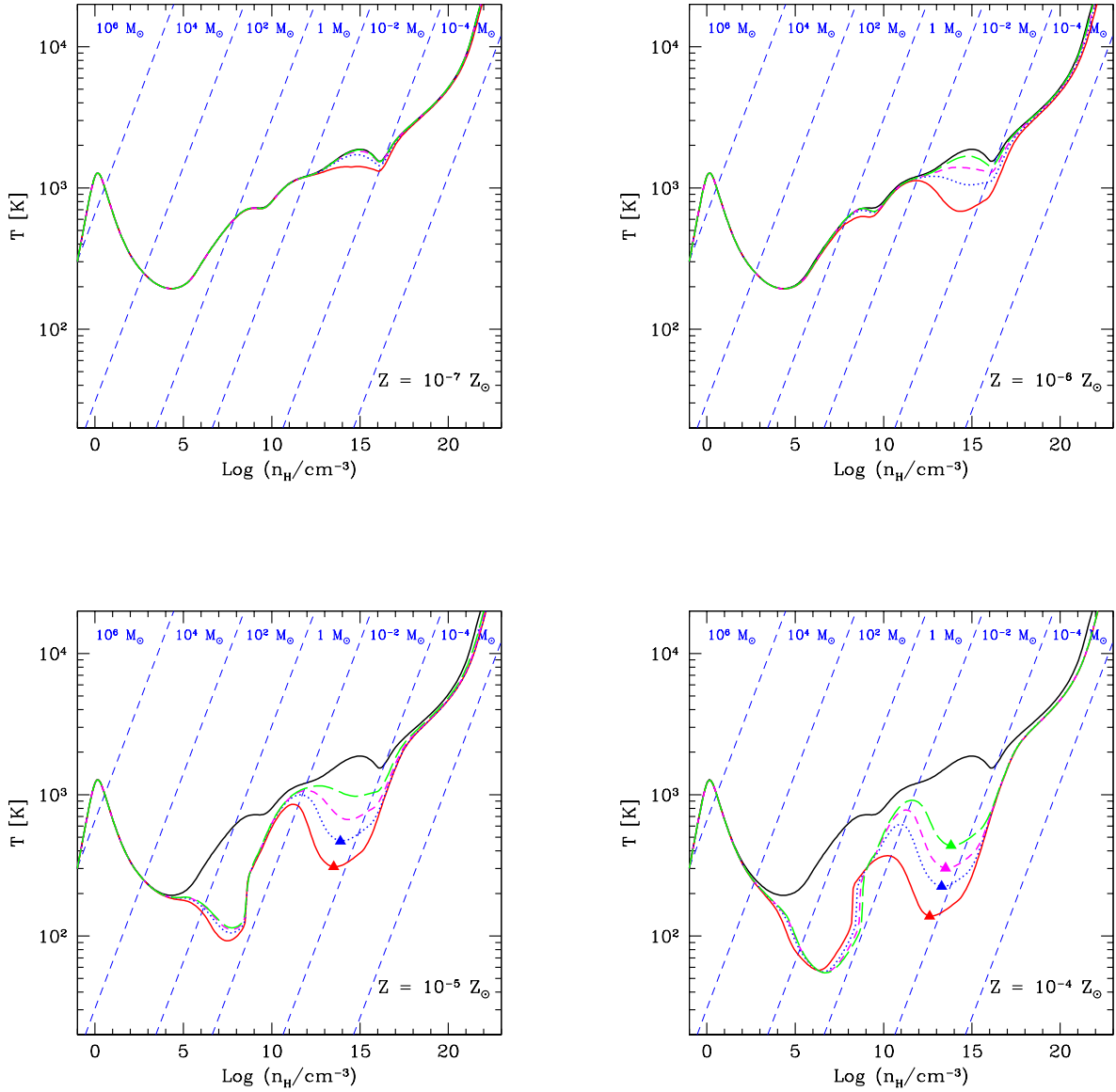


Figure 7. Same as Fig. 6 but for the $(20M_{\odot}, 10^{-4}Z_{\odot})$ SN model.

be inferred from the last column of Table 1, differences in S among different reverse shock models for a given SN progenitor are less than 15%. Taking S to vary in the range $2.22 \leq S/10^5 \text{cm}^2/\text{gr} \leq 5.37$, the condition on the dust-to-gas ratio reads,

$$\mathcal{D} > [2.6 - 6.3] \times 10^{-9} \left[\frac{T}{10^3 \text{K}} \right]^{-1/2} \left[\frac{n_{\text{H}}}{10^{12} \text{cm}^{-3}} \right]^{-1/2}, \quad (17)$$

consistent with value of \mathcal{D}_{cr} inferred above and drawn in the figure.

It is important to stress that this simple analytic argument is not able to capture all the important details of the evolution which may activate dust-induced fragmentation. In particular, the condition that $\gamma < 0.8$ during the

dust-induced cooling phase depends also on the grain opacity: if we increase the dust opacity for fixed surface area, the dust-gas coupling temperature becomes lower, leading to a deeper dip in the equation of state.

In addition, the fragmentation criteria that we follow ($\gamma > 0.97$ after a phase of cooling where $\gamma < 0.8$) have been established through a comparison with numerical studies (Tsuribe & Omukai 2006; Omukai et al. 2010). It is clear that the process of fragmentation does not depend only on the gas thermal evolution, being influenced also by the detailed hydrodynamical properties of the clouds, such as the initial amplitude of fluctuations, rotation and turbulence. Thus, our study can provide a guideline for more sophisticated numerical simulations.

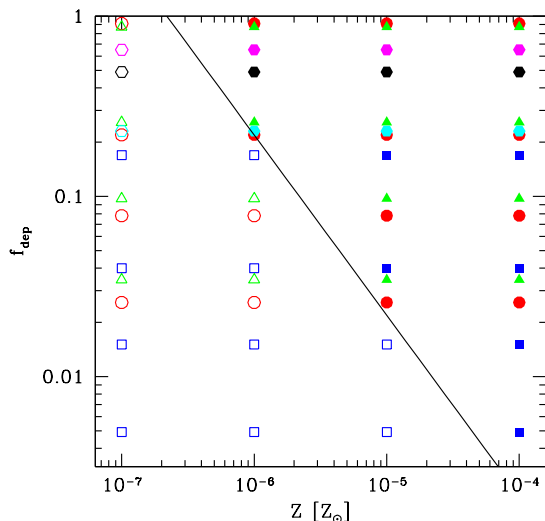


Figure 8. Fragmentation (filled symbols) and no-fragmentation (empty symbols) conditions for each considered SN progenitors and reverse shock model. Red circles, blue squares, and green triangles refer to $(20M_{\odot}, 0)$, $(20M_{\odot}, 10^{-4}Z_{\odot})$, and $(35M_{\odot}, 10^{-4}Z_{\odot})$ models, respectively. In addition, we also show the SN and PISN models analyzed in Schneider et al. (2006, cyan and magenta exagons) and the model which adopts local ISM conditions as in Omukai et al. (2005, black exagon). The black solid line shows the predicted behaviour for a constant dust-to-gas ratio of $\mathcal{D}_{\text{cr}} = 4.4 \times 10^{-9}$ (see text).

6 DISCUSSION

Although we have considered only star-forming regions in the first mini-halos, metals and dust rapidly enrich more massive halos, with masses $M \sim 10^8 M_{\odot}$ at $z \sim 10$, the so-called first galaxies (Bromm & Yoshida 2011). When the gas is accreted onto these halos, it is shock-heated at the virial radius of the parent dark matter halo to virial temperatures $T_{\text{vir}} \sim 10^4$ K; then it cools via the atomic-hydrogen Lyman- α line, falling inward and attaining increasingly larger densities. In Schneider et al. (2002), we investigate the dependence of thermal evolution of collapsing gas clouds on the initial virial temperature (halo mass). For metal-free gas, the evolution with temperature of the ionization fraction and of the fraction of molecular hydrogen is independent of the halo virial temperature. If the gas is fully ionized, molecules form through nonequilibrium recombination, leading to overall fractions that are much higher than in the expanding homogeneous universe (Uehara & Inutsuka 2000). As a consequence of enhanced H_2 and HD fractions, the gas rapidly cools to the CMB temperature and $\sim 10M_{\odot}$ fragments are formed (Johnson & Bromm 2006).

In the presence of a strong LW background, the gas in the first galaxies remains free of H_2 (Omukai 2001), it avoids fragmentation and leads to the formation of a single super-massive star with mass as high as $\sim [10^5 - 10^6]M_{\odot}$, which then evolves into a super-massive black hole (Bromm & Loeb 2003b). Omukai, Schneider & Haiman (2008) find that, even in these systems, fragmentation is inevitable when

the gas is pre-enriched above a critical metallicity, whose value is between $3 \times 10^{-2}Z_{\odot}$ (in the absence of dust) and as low as $5 \times 10^{-6}Z_{\odot}$ (with a dust-to-gas mass ratio of about $0.01Z/Z_{\odot}$).

Recently, Dekel & Birnboim (2006) and Dekel et al. (2009) have proposed an alternative accretion mode, the so-called ‘cold accretion’: gas falls in the halos along cosmic filaments and it is deposited much closer to the center of the galaxy, at much higher densities. In these conditions, the fragmentation properties of the gas are likely to be modified. Safranek-Shrader, Bromm & Milosavljević (2010) find that H_2 and HD dominate gas cooling at $T < 10^3$ K and metallicity has no effect on fragmentation. In the presence of a strong LW background which photo-dissociates H_2 , metal-line cooling becomes important and, when the metallicity is $Z \sim 10^{-4}Z_{\odot}$, $\sim 3M_{\odot}$ fragments are formed. While this appears an interesting possibility to form low-mass stars, the final fragmentation mass depends sensitively on the adopted initial gas density. Thus, a larger set of initial conditions needs to be investigated to draw robust conclusions.

Finally, it is important to mention the effects of the CMB radiation field on the thermal evolution of collapsing gas clouds, which have not been included in the present study. In general, the presence of the CMB radiation field is important at high redshifts and metallicities (Smith et al. 2009), inhibiting fragmentation. Schneider & Omukai (2010) find that in the absence of dust grains, the fragmentation mass scales at $z > 10$ are always $\geq 100s$ of M_{\odot} , independent of the gas initial metallicity. When $Z < 10^{-2}Z_{\odot}$, dust-cooling remains relatively insensitive to the presence of the CMB, and sub-solar mass fragments are formed at any redshift. It is only when $Z > 10^{-2}Z_{\odot}$ and $z > 10$ that the heating of dust grains by the CMB starts to inhibit the formation of sub-solar mass fragments (Schneider & Omukai 2010). Thus, the conclusions of the present study remain valid in all but these extreme conditions.

7 CONCLUSIONS

In this study, we have explored the conditions which enable the formation of solar and sub-solar mass fragments during the collapse of pre-enriched gas clouds within the first mini-halos at $z \sim 20 - 30$.

By carefully analysing the thermal and chemical evolution of star-forming clouds, we find that in the absence of dust grains, gas fragmentation occurs at densities $n_{\text{H}} \sim [10^4 - 10^5] \text{cm}^{-3}$ when the metallicity exceeds $Z \sim 10^{-4}Z_{\odot}$. The resulting fragmentation masses, identified by the minimum Jeans mass at the fragmentation epoch, are $\geq 10M_{\odot}$. The inclusion of Fe and Si cooling (which can dominate metal-line emission in some density ranges) does not affect the thermal evolution as this is dominated by molecular (mostly OH, H_2O and CO) cooling even for metallicities as large as $Z = 10^{-2}Z_{\odot}$.

The presence of dust is the key driver for the formation of solar-mass stars. We have explored the fragmentation properties of collapsing clouds pre-enriched with dust and metals synthesized by core-collapse SNe. Focusing on three representative SN progenitors (a $Z = 0$ star with $20M_{\odot}$ and two $Z = 10^{-4}Z_{\odot}$ stars with $20M_{\odot}$ and $35M_{\odot}$), we compute the mass of dust and metals (hence the depletion

factor), grain composition and size distribution using the model by Bianchi & Schneider (2007). To determine the minimum dust depletion factor required to activate dust-driven fragmentation, we start from the above initial conditions and consider the effects of SN reverse shocks of increasing strength: these reduce the depletion factors, alter the shape of the grain size distribution function and modify the relative abundances of grain species and of metal species in the gas phase. Following this approach, we can control all these effects in a self-consistent way and explore the implications for the fragmentation properties of pre-enriched star forming clouds.

We find that the lowest metallicity at which fragmentation occurs is $Z = 10^{-6}Z_{\odot}$ for gas pre-enriched by the explosion of a $20M_{\odot}$ primordial SN and/or by a $35M_{\odot}$, $Z = 10^{-4}Z_{\odot}$ SN; it is ~ 1 dex larger, when the gas is pre-enriched by a $Z = 10^{-4}Z_{\odot}$, $20M_{\odot}$ SN. In both cases, however, cloud fragmentation depends on the depletion factor and it is suppressed when the reverse shock leads to a too large destruction of dust grains.

These features are all consistent with the idea that there is a minimum dust-to-gas ratio, \mathcal{D}_{cr} , above which fragmentation is activated. By requiring that the energy transfer rate between gas and dust is larger than the compressional heating rate, we derive a simple analytic expression for \mathcal{D}_{cr} which depends on the total grain cross-section per unit mass of dust; for grain composition and properties explored in the present study, this critical dust-to-gas ratio is $\mathcal{D}_{\text{cr}} = [2.6 - 6.3] \times 10^{-9}$. When the dust-to-gas ratio of star forming clouds exceeds this value, the fragmentation masses range between $0.01M_{\odot}$ and $1M_{\odot}$, thus enabling the formation of the first low-mass stars.

According to this criterium, the recently observed Galactic Halo star with a total metallicity of $Z = 4.5 \times 10^{-5}Z_{\odot}$ (Caffau et al. 2011) requires a minimum dust depletion of $f_{\text{dep}} \geq (4-9) \times 10^{-3}$ in the parent gas cloud, consistent with the values predicted for ordinary core-collapse SN investigated in the present study.

ACKNOWLEDGMENTS

We gratefully acknowledge all members of the DAVID collaboration (www.arcetri.astro.it/david) for inspiration and stimulating discussion. The present work is supported in part by the Grants-in-Aid by the Ministry of Education, Science and Culture of Japan (2168407, 21244021:KO).

REFERENCES

- Abel T., Brian G. & Norman M. L. 2002, *Science*, 295, 93
- Anders, E., & Grevesse, N. 1989, *Geochimica et Cosmochimica Acta*, 53, 197
- Bastian N., Covey K. R., Meyer M. R. 2010, *ARA&A*, 48, 339
- Bianchi S. & Schneider R. 2007, *MNRAS*, 378, 973
- Beers T. C. & Christlieb N. 2005, *ARA&A*, 43, 531
- Bromm V., Ferrara A., Coppi P. & Larson R. B. 2001, *MNRAS*, 328, 969
- Bromm V., Coppi P. & Larson R. B. 2002, *ApJ*, 564, 23
- Bromm V., Loeb A. 2003, *Nature*, 425, 812
- Bromm V., Loeb A. 2003b, *ApJ*, 596, 34
- Bromm V., Loeb A. 2004, *New Astronomy*, 9, 353
- Bromm V., Yoshida N., Hernquist L., McKee C. F. 2009, *Nature*, 459, 49
- Bromm V. & Yoshida N., 2011, *ARA&A*, in press [eprint arXiv:1102.4638]
- Caffau, E. et al. 2011, *Nature*, 477, 67
- Clark P. C., Glover S. C. O., Klessen R. S. 2008, *ApJ*, 672, 757
- Clark P. C., Glover S. C. O., Smith R. J., Greif T. H., Klessen R. S., Bromm V. 2011, *Science*, 331, 1040
- Clark P. C., Glover S. C. O., Klessen R. S., Bromm V. 2011b, *ApJ*, 727, 110
- Clarke C. J. & Bromm V. 2003, *MNRAS*, 343, 1124
- Dekel A. & Birnboim Y. 2006, *MNRAS*, 368, 2
- Dekel A. et al. 2009, *Nature*, 457, 451
- Dopcke G., Glover S. C. O., Clark P. C., Klessen R. S. 2011, *ApJ*, 729, L3
- Elmegreen B. G., Klessen R. S. & Wilson C. D. 2008, *ApJ*, 681, 365
- Elmegreen B. G. 2009, in "The Evolving ISM in the Milky Way and Nearby Galaxies", The Fourth Spitzer Science Center Conference, eds. K. Sheth, A. Noriega-Crespo, J. Ingalls, and R. Paladini, Published online at <http://ssc.spitzer.caltech.edu/mtgs/ismevol/>
- Frebel A., Johnson J.L., Bromm V. 2007, *MNRAS*, 380, L40
- Greif T. H., Springel V., White S. D. M., Glover S. C. O., Clark P. C., Smith R. J., Klessen R. S. & Bromm V. 2011, *ApJ*, in press [eprint arXiv:1101.5491]
- Helmi A. 2008, *ARA&A*, 15, 145
- Hocuk S., Spaans M. 2010, *A&A*, 510, 110
- Hosokawa T., Omukai K. 2009, *ApJ*, 703, 1810
- Jappsen A. K., Klessen R. S., Larson R. B., Li Y., Mac Low M. M. 2005, *A&A*, 435, 611
- Jappsen A. K., Glover S. C. O., Klessen R. S., Mac Low M. M. 2007, *ApJ*, 660, 1332
- Jappsen A. K., Mac Low M. M., Glover S. C. O., Klessen R. S., Kitsionas S. 2009, *ApJ*, 694, 1161
- Jarosik N. et al. 2011, *ApJS*, 192, 14
- Johnson J. L. & Bromm V. 2006, *MNRAS*, 366, 247
- Kozasa, T., Hasegawa, H. & Nomoto, K. 1989, *ApJ*, 344, 325
- Larson R. B. 2005, *MNRAS*, 359, 211
- Li Y., Klessen R. S., Mac Low M.-M., 2003, *ApJ*, 592, 975
- Machida M. N., Omukai K., Matsumoto T., Inutsuka I. 2008, *ApJ*, 677, 813
- Machida M. N., Omukai K., Matsumoto T., Inutsuka I. 2009, *MNRAS*, 399, 1255
- McKee C. F., Tan J. 2008, *ApJ*, 681, 771
- Ohkubo T., Nomoto K., Umeda H., Yoshida N., Tsuruta S. 2009, *ApJ*, 706, 1184
- Omukai K. 2000, *ApJ*, 534, 809
- Omukai K. 2001, *ApJ*, 546, 635
- Omukai K., Palla F. 2003, *ApJ*, 589, 677
- Omukai K., Tsuribe T., Schneider R., Ferrara A. 2005, *ApJ*, 626, 627
- Omukai K., Schneider R. & Haiman Z. 2008, *ApJ*, 686, 801
- Omukai K., Hosokawa T., Yoshida, N. 2010, *ApJ*, 722, 1793
- Pollack, J. B., Hollenbach, D., Beckwith, S., Simonelli, D. P., Roush, T., Fong, W. 1994, *ApJ*, 421, 615
- Raiteri C. M., Villata M., Navarro J.F. 1996, *A&A*, 315, 105
- Safrank-Shrader C., Bromm V. & Milosavljević M. 2010, *ApJ*, 723, 1568
- Santoro F. & Shull M. J. 2006, *ApJ*, 643, 26
- Schneider R., Ferrara A., Natarajan P., Omukai K. 2002, *ApJ*, 571, 30
- Schneider R., Ferrara A., Salvaterra R., Omukai K., Bromm V. 2003 *Nature*, 422, 869
- Schneider, R., Ferrara, A. & Salvaterra, R. 2004, *MNRAS*, 351, 1379
- Schneider R., Omukai K., Inoue A. K., Ferrara A. 2006, *MNRAS*, 369, 1437

- Schneider R., Omukai K. 2010, MNRAS, 402, 429
Schleicher D. R. G., Galli D., Glover S. C. O., Banerjee R., Palla F., Schneider R., Klessen R. S. 2009, ApJ, 703, 1096
Smith B. D., Sigurdsson S. & Abel T. 2008, MNRAS, 385, 1443
Smith B. D., Turk M. J., Sigurdsson S., O'Shea B. W., Norman M. L. 2009, ApJ, 691, 441
Stacy A., Greif T. H., Bromm V. 2010, MNRAS, 403, 45
Tan J., McKee C. F. 2004, ApJ, 603, 383
Todini, P. & Ferrara, A. 2001, MNRAS, 325, 726
Tsuribe T., Omukai K., 2006, ApJ, 642, 61
Tsuribe T., Omukai K., 2008, ApJ, 676, L45
Turk M. J., Abel T., O'Shea B. 2009, Science, 325, 601
Uehara H. & Inutsuka S. 2000, ApJ, 531, L91
Yoshida N., Omukai, K., Hernquist, L. & Abel, T. 2006, ApJ, 652, 6
Yoshida N., Omukai K. & Hernquist L. 2008, Science, 321, 669